RANDOM-MODULATION CW LIDAR SYSTEM FOR SPACE-BORNE CARBON DIOXIDE REMOTE SENSING BASED ON A HIGH-BRIGHTNESS SEMICONDUCTOR LASER

I. Esquivias[1], A. Pérez-Serrano[1], J.M.G. Tijero[1], M. Faugeron[2], F. van Dijk[2], M. Krakowski[2], G. Kochem[3], M. Traub[3], J. Barbero[4], P. Adamiec[4], X. Ai[5], J. Rarity[5], M. Quatrevalet[6], G. Ehret[6]

[1]Universidad Politécnica de Madrid, ETSI Telecomunicación-CEMDATIC, Spain. [2] III-V Lab Campus Polytechnique, France. [3] Fraunhofer Institute for Laser Technology ILT, Germany. [4]Alter Technology TÜV Nord S.A.U., Spain. [5] University of Bristol, Department of EEE, United Kingdom. [6] Institut für Physik der Atmosphäre, DLR, Germany.

I. INTRODUCTION

The accurate determination of the atmospheric distribution of carbon dioxide (CO_2) on planetary scale is a key requirement for setting up modeling tools able to make reliable predictions of Earth climate dynamics which are essential for the understanding of such important issues as climate change and global warming. Nowadays, the concentrations of CO_2 are mainly measured in-situ at a number of surface stations that are unevenly distributed over the planet. Air-borne and space-borne missions have the potential to provide a denser and better distributed set of observations to complement those provided by the surface network.

In the framework of the European Project BRITESPACE [1], we have proposed an all-semiconductor laser source for an Integrated Path Differential Absorption (IPDA) LIDAR for column-averaged measurements of atmospheric CO_2 in future space missions [2].

Pulsed IPDA LIDAR systems, such as the CO_2 and CH_4 Atmospheric Remote Monitoring-Flugzeug (CHARM-F) [3] estimate the column concentration of greenhouse gases in the atmosphere by looking at the back-scattered pulse echoes at the end of the optical path, which is either the cloud top or the Earth's surface (see Fig. 1(a)). The term 'differential absorption' refers to the difference of the absorption of a pair of laser lines with slightly different wavelengths: the on-line wavelength is near the center of a CO_2 absorption line while the off-line wavelength is set close to but off the same absorption line (see Fig 1 (b)). Both wavelengths are close enough such that the two lines exhibit almost identical aerosol attenuation but obviously different CO_2 absorption. Hence, the relative absorption by the CO_2 molecules can be calculated by the power ratio of the back-scattered signals at the end of the optical path and it can be converted into a column-averaged mixing ratio thanks to the knowledge of the path length from the round-trip time delay. However, to avoid the ambiguity between the returned on-line and off-line pulse pairs, the temporal separation between these two pulses must be set to more than the round-trip time from the top of the atmosphere to ground. This results in a misalignment of the footprints of the pulse pairs which deteriorates detection accuracy due to the associated ground reflectance and altitude variations.

Random-modulation CW (RM-CW) LIDAR [4] is capable of obtaining range gated back-scattering information as obtained from pulsed techniques. It has been applied in Differential Absorption LIDAR (DIAL) measurements [5], and its distance precision has been recently enhanced [6]. In RM-CW LIDAR, a pseudo-random binary sequence (PRBS) is transmitted. The received signal correlated with the original PRBS code gives a range resolved response with a non-ambiguous range determined by the number of PRBS bits (repetition rate) which can be extended further than the trip time corresponding to the atmosphere thickness. Overall, the average power of a RM-CW system would be increased beyond that of a typical pulsed system which will be limited by damage effects and nonlinear frequency drift at high peak powers. Hence, although there is a slight signal to noise (SNR) reduction in RM-CW systems due to ambient shot noise [7], the increased numbers of photons sent should amply compensate for this deficiency. The auto-correlation property of the PRBS and the temporal shifting of the codes can be used to transmit both wavelengths simultaneously, which avoids the beam misalignment problem (see Fig. 1(c)). Furthermore, due to the extended non-ambiguity distance, equals to the total PRBS code length, the returns can be binned into different range gates with the distance resolution limited by the PRBS bit time (chip time). Its potential for IPDA LIDAR has also been recently recognized in [8] where PRBS modulation has been adapted to Laser Absorption Spectroscopy systems.

The availability of suitable laser sources is one of the main challenges in future space missions for atmospheric remote sensing. Typical laser sources currently used in DIAL systems are solid state lasers working in pulsed regime and emitting ns pulses with high energy at low to medium repetition rate (typical values are 10-50 ns, ~10-50 mJ, 50-200 Hz) [9, 10]. Although these laser systems have demonstrated the high average power and the high laser beam quality and frequency stability required by the application, it is at the expense of a bulky system with low wall plug efficiency, which is a main concern for space-borne applications. Hybrid Master Oscillator Power Amplifiers (MOPAs) combining a Distributed Feedback (DFB) semiconductor laser as

seed laser and Erbium Doped Fiber Amplifiers (EDFAs) working in pulsed conditions have been investigated in the context of NASA mission ASCENDS [11]. However, the use of active optical fibers in space applications requires specific attention to the radiation shielding, the orbit and the duration of the flight, since it is known that fiber amplifier materials have low radiation hardness [12]. All-semiconductor laser sources are very interesting candidates for space-borne atmospheric sensing applications, due to their compactness, high efficiency, reliability, and radiation hardness. They cannot produce the high energy pulses needed in standard pulsed IPDA LIDAR, but they are very well suited to RM-CW systems.

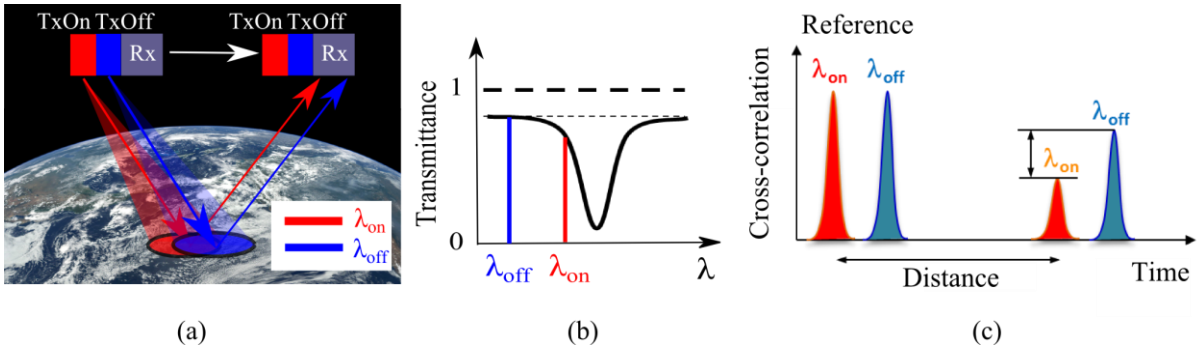

Fig. 1. (a) Illustration of the space-borne instrument in operation. (b) Typical CO_2 transmittance curve, with the on-line and off-line wavelengths denoted. (c) Cross-correlation between the sent and received signals allowing the distance measurement.

In this paper, we report on the progresses of BRITESPACE Consortium in the design of the laser transmitter and the IPDA LIDAR system (Section II). Results on the experimental characterization of the laser source based on a high brightness all-semiconductor tapered MOPA are provided in Section III. Theoretical calculations of the system performance are reported in Section IV and finally, a brief summary is given in Section V.

II. LASER TRANSMITTER AND SYSTEM DESIGN

The design of the complete IPDA LIDAR system is shown in Fig. 2 (a). It consists of the laser transmitter, the optics for beam transmission and reception and the control electronics. Specifically, the output beam from the transmitter is split in two branches: one is sent to the beam expander and then to the atmosphere and the other is used as reference in the comparison with the received signal, for the calculation of CO_2 concentration. The reflected light from Earth ground is collected by a reflective telescope with a Field of View (FOV) matching the laser beam divergence and alignment issues are addressed by using a short wave infrared (SWIR) camera.

A very high sensitivity detector based on InGaAs negative feedback avalanche diodes (NFAD) is proposed for single photon counting of the received signal [13]. The modulation sequence and the correlation process required by the RM-CW technique are implemented with a Field Programmable Gate Array (FPGA).

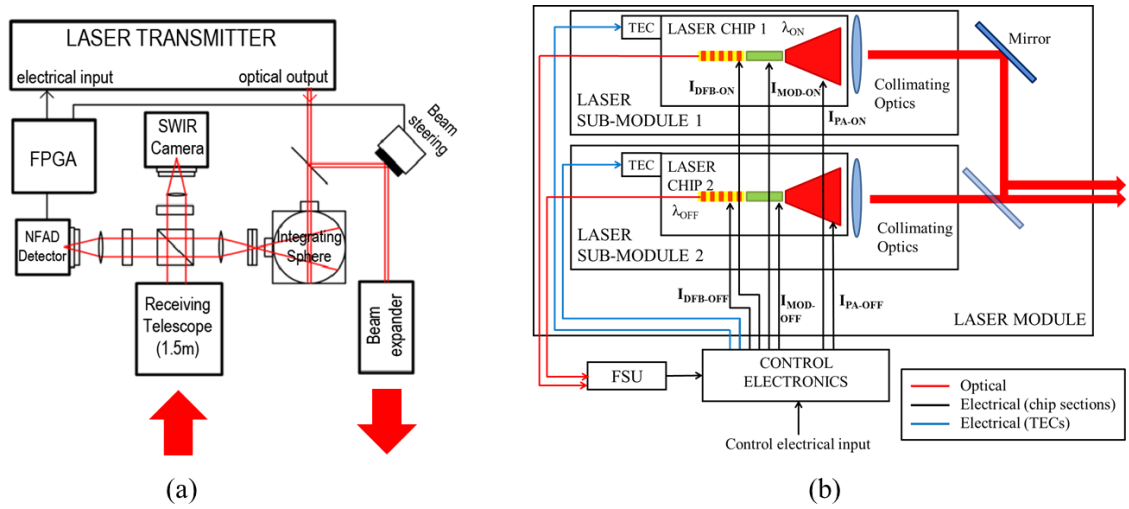

Fig. 2. (a) Block scheme of the complete IPDA LIDAR system. (b) Block scheme of the laser transmitter.

The laser transmitter architecture is shown in Fig. 2 (b). It consists of two space compatible laser sub-modules, the control electronics and the Frequency Stabilization Unit (FSU). Two laser chips, one for each sounding frequency (λ_{On}, λ_{Off}) required for CO_2 detection in IPDA systems, are housed in the laser module, together with the beam forming optics and two power monitoring photodiodes. The back facet output of the laser chips are sent to the FSU through standard Single Mode Fibers (SMF) for frequency stabilization. In the following, laser module and FSU are described in detail.

A. Laser module

For each laser chip, a sub-module has been designed in order to provide electrical access, temperature control and beam forming optics for each tapered MOPA. Fig. 3 (a) shows the design of the laser module; Fig. 3 (b) and (c) show photographs of a real sub-module with a working MOPA without the collimating optics. The radiation emitted by the tapered amplifier is astigmatic, i.e. it has different virtual sources (and different angles of divergence) for the fast axis (vertical direction) and for the slow axis (horizontal direction). Due to this characteristic an optical system for the collimation of a tapered amplifier must consist of two lenses. We propose the use of a first aspheric lens and a second cylindrical lens. The first lens is for collimation of the fast axis and intermediate focusing of the slow axis while the second cylindrical lens collimates the slow axis without affecting the fast axis beam. Considering also the bended geometry of the laser chips (see Section III below), the emitter is tilted in the slow axis in order to achieve perpendicular propagation.

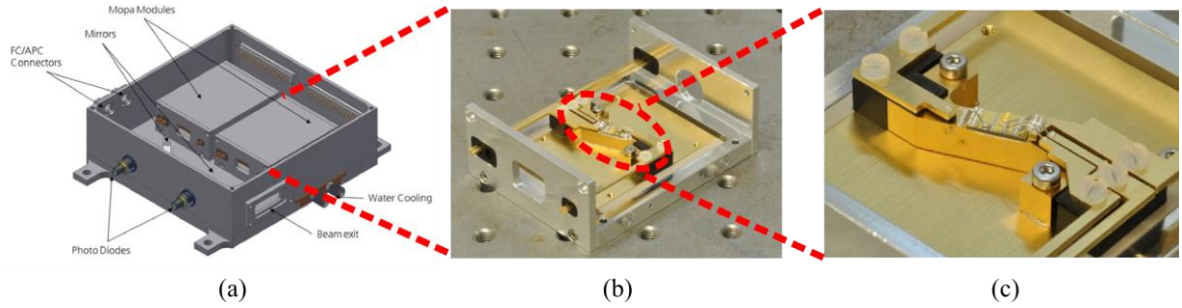

Fig. 3. (a) Design of the laser module. (b) Photograph of the laser sub-module without the collimating optics. (c) Photograph of the mounted laser chip.

The radiation emitted from the back facet of the DFB is expected to be diffraction limited, and therefore can be coupled into a lensed Single Mode Fiber (SMF) aligned to the DFB back facet.

Two mirrors, one for each sub-module, are used for combining the output beams before exiting the laser module. Partially reflective mirrors will be used in order to allow power monitoring for each MOPA with two photodiodes placed right after the combining mirrors. The laser beams from the two laser chips are placed close each other at the laser module output, for minimizing footprint errors in IPDA detection.

B. Frequency stabilization unit

For accurate estimation of gas molecule concentration IPDA lidar systems require high frequency stabilization, in order to have precise measurement of the detected power ratio at the selected absorption line [2]. Fig. 4 shows the absorption lines for CO_2 and H_2O. The proposed absorption line is the line at 1572 nm. It has been chosen because of its high absorption and low interference from the H_2O lines. The on and off-line frequencies are detailed in Table 1, as well as the spectral requirements, based on estimations of the error budget.

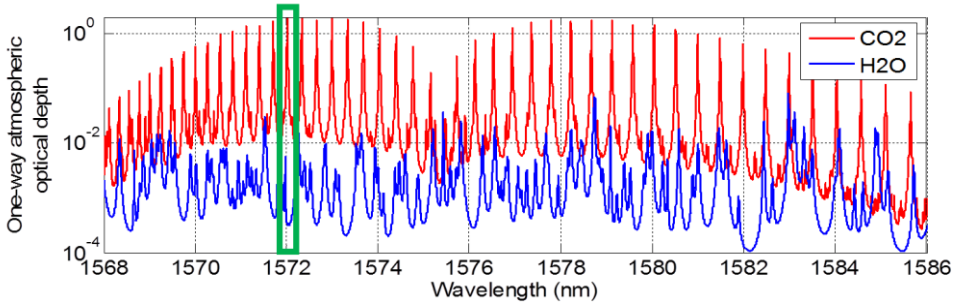

Fig. 4. CO_2 spectrum (red line) and H_2O spectrum (blue line). The green box indicates the proposed absorption line for the project BRITESPACE (same as in the project CHARM-F).

Regarding frequency stability and knowledge accuracy (see Table 1), the most critical is the on-line frequency, due to the slope in the wing of the line (see Fig. 1 (b)). The linewidth and linewidth knowledge accuracy is expected to be uncritical for the BRITESPACE transmitter, because pseudo-random modulation dominates the linewidth which is therefore well known.

Channel	Nominal frequency (THz)	Tunability (MHz)	Long term frequency stability/knowledge accuracy (MHz)	
			Maximum	Desirable
On-line	190.704710	± 350 MHz	0.1	0.02
Off-line	190.694980	N/A	100	20

Table 1. Nominal frequencies for channels on- and off-line; and frequency requirements.

In order to achieve these frequency requirements, we propose the use of two opto-electrical feedback loops for the stabilization of the on- and off-channels coupled to the output of a third opto-electrical feedback loop for CO_2 locking. A scheme, showing the selected design for the FSU, is shown in Fig. 5.

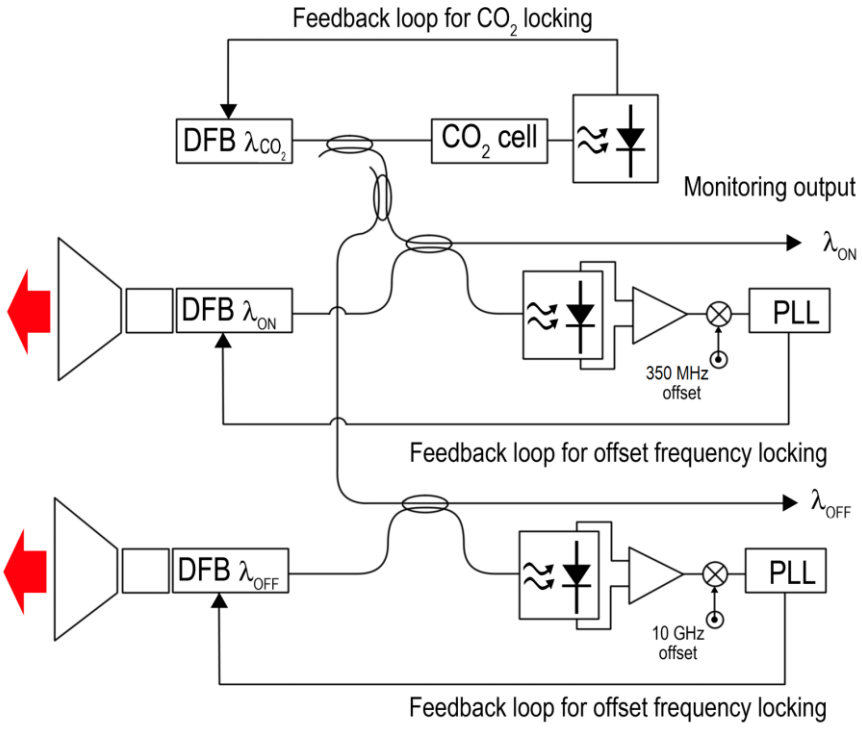

Fig. 5. Block scheme of the frequency stabilization unit. PLL: Phase Locked Loop.

Light emitted from the back facet of the DFB section of the on-line MOPA will be collected through a lensed SMF fiber and sent to a fiber coupler. One of the output ports of the coupler will be sent to the on-line locking feedback loop and the other will be used for monitoring. In the same way, the light emitted from the back facet of the off-line MOPA will be sent to a second fiber coupler. One of the outputs will be sent to the off-channel locking feedback loop while the other will be used for monitoring.

We will use a master DFB laser that will be locked to the selected CO_2 absorption line using a multi pass CO_2 reference cell and a custom feedback loop based on a commercially available (LaseLock, TEM Messtechnik GmbH) laser frequency locking equipment. The light emitted from the master laser will be injected into the on- and off-line frequency locking loops and it will be used to stabilize the beat note of the on- and off-line signals with respect to the master laser frequency, with a tunable 350 MHz and with a fixed 10 GHz offsets, respectively.

III. EXPERIMENTAL RESULTS

InGaAsP/InP monolithic MOPAs were fabricated as the main building block of the laser transmitter. Each MOPA is a three section device, consisting of a frequency stabilized DFB master oscillator, a modulator section,

and a tapered amplifier. The use of this original structure aims to fulfill the performances required by the IPDA system in terms of high power, frequency stability and good beam quality. The DFB section is accurately frequency stabilized by an external opto-electrical feedback loop through the FSU (see Section II.B.). The modulator section is introduced for implementation of the RM-CW technique in the proposed IPDA system. Finally, the geometry of the tapered amplifier is optimized in order to provide high brightness output beam with sufficient power and beam quality.

Three different geometries were initially proposed and fabricated for the laser chip implementation, based on i) straight, ii) tilted, and iii) bended designs. The tilted and bended geometries were proposed in order to minimize undesired optical feedback from the amplifier section to the DFB oscillator. In fact, standard straight monolithically integrated MOPAs exhibit instabilities due to compound cavity effects arising from the residual reflectivity at the amplifier output facet [14, 15]. The best experimental results in terms of output power and spectral quality were obtained for the bended geometry shown in Fig. 6 (a). Fig. 6 (b) shows a photograph of the bended MOPA where the different contacts for the three sections and the thermistor contact for temperature control can be observed.

The measured CW output power vs. amplifier current characteristics for a bended MOPA are shown in Fig. 6 (c) for different modulator section currents and a DFB current fixed at 400 mA. The maximum optical power of around 400 mW corresponds to a modulator current of 300 mA. The static Extinction Ratio (ER) when switching the modulator current between 0 and 300 mA is 26 dB.

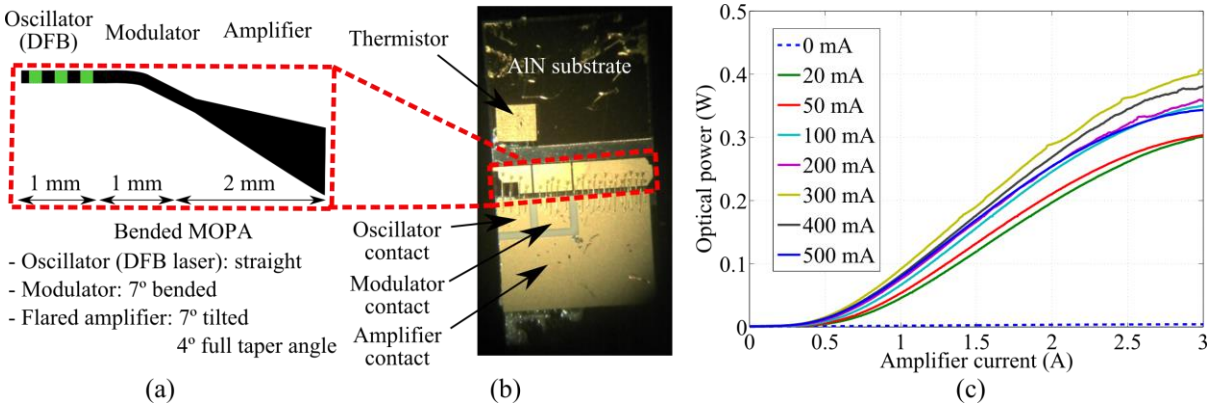

Fig. 6. (a) Scheme of the bended MOPA. (b) Photograph of the bended MOPA showing the contacts of each section. (c) Experimental L-I curves of the bended MOPA for different values of the modulator current. The pump current of the oscillator (DFB) is fixed to 400 mA.

Fig. 7 (a) shows the optical spectra for different modulator currents. Single frequency operation with Side Mode Suppression Ratio (SMSR) around 50 dB is apparent. The peak wavelength shows high stability when changing the modulator current, with a maximum shift of 40 pm, as it can be observed in Fig. 7 (b). This shift is attributed to cross-heating effects in static conditions, but it is not expected at the proposed modulation rate of 25 Mbps.

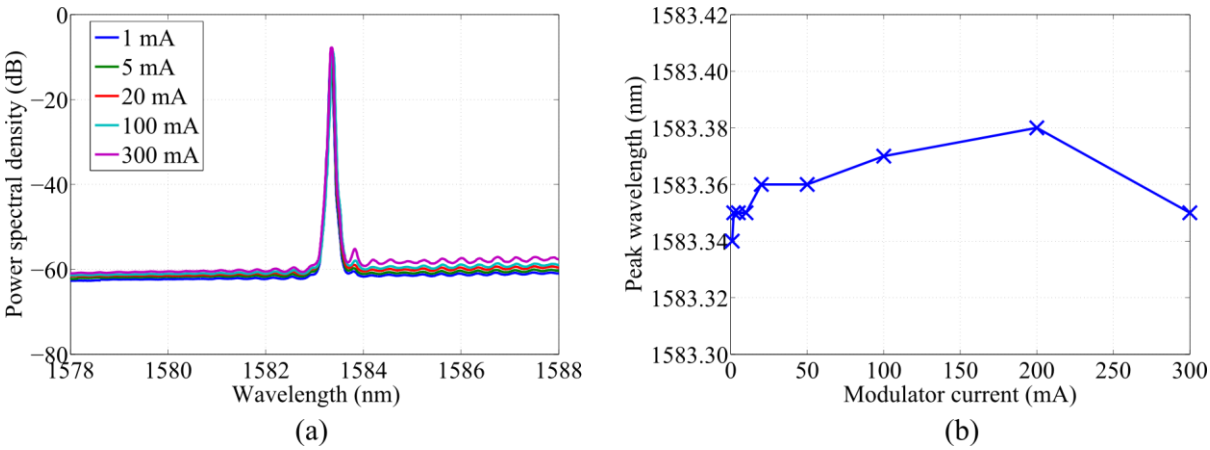

Fig. 7. (a) Optical spectra for different current values of the modulator section. The pump current of the oscillator (DFB) is fixed at 400 mA, while the pump current of the amplifier is fixed at 3 A. (b) Peak wavelength of the optical spectra shown in (a) for the different modulator currents.

IV. THEORETICAL RESULTS

In this section the noise performance of the system in space-borne scenarios is investigated. It has been identified that the major noise contributions in the proposed system will come from the signal/ambient shot noise and detector dark noise. Details on the derivation of the following model can be found in [13]. The Signal to Noise Ratio (SNR) of the RM-CW system can be calculated as

$$SNR_{on,off} = \frac{N_{on,off}}{\sqrt{2\,(N_{on,off} + N_{off,on} + m\,(N_{amb} + N_{det}))}}, \tag{1}$$

where $N_{on,off}$ are the on- and off-line number of photoelectrons integrated in their range gate respectively, $m\ N_{amb}$ is the number of photoelectrons due to the ambient and $m\ N_{det}$ is the number of photoelectrons due to the detector. They can be calculated with the following expressions,

$$N_{on,off} = P_{on,off}^{avg}\ T_{int}\ \eta_0\ \frac{\alpha_S}{\pi} T_{on,off}\ \frac{A_r}{R^2}\xi_e, \tag{2}$$

$$mN_{amb} = m\ T_C\ \eta_0\ \Delta\lambda\ L_r \left(\frac{\theta_{FOV}\ R}{2}\right)^2 \frac{A_r}{R^2}\xi_e, \tag{3}$$

$$mN_{det} = m\ T_C\ N_{dc}, \tag{4}$$

where the different parameters are described and given in Table 2 and $\xi_e = \eta_e \lambda_{on}/hc$ is the photon energy. The number of 1s in the PRBS signal during the integration time m is calculated considering Non-Return to Zero (NRZ) format as $m = T_{int}/2T_C$. Finally one can write the CO_2 mixing ratio precision as

$$\sigma_{XCO_2} = \frac{XCO_2}{2\ DAOD}\sqrt{\left(SNR_{on}\right)^{-2} + \left(SNR_{off}\right)^{-2}}. \tag{5}$$

For the parameters given in Table 2, σ_{XCO_2} = 1.5 ppm, which is the target observational requirement taken from [16]. Fig. 8 (a) shows the σ_{XCO_2} dependence on the on- and off-line average powers (assuming that both are the same) for different values of the bandpass filter FWHM. As expected, for narrower filters one obtains better precision (below the target requirement of 1.5 ppm) for average powers of a few Watts. The filter FWHM is limited by the separation between the on- and off-wavelengths. The dependence of σ_{XCO_2} on the orbit altitude is shown in Fig. 8 (b). It exhibits a linear behavior, whose slope is given by the different bandpass filter FWHM.

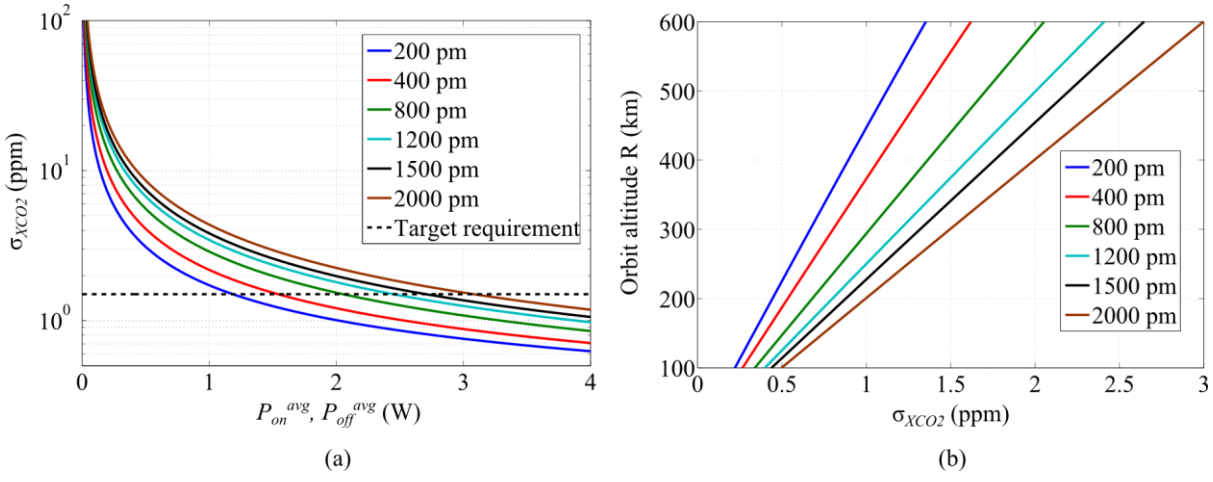

Fig. 8. (a) σ_{XCO_2} dependence on $P_{on}^{avg} = P_{off}^{avg}$, for different values of the bandpass filter FWHM, $\Delta\lambda$. (b) σ_{XCO_2} dependence on the orbit altitude of the system for different values of the bandpass filter FWHM, $\Delta\lambda$. The values of the rest of the parameters are given in Table 2.

Description	*Symbol*	*Value*	*Units*
Transmitter			
On-line average power	P_{on}^{avg}	2	W
Off-line average power	P_{off}^{avg}	2	W
Chip (bit) time	T_C	40	ns
Integration time	T_{int}	7	s
On-line wavelength	λ_{On}	1572.02	nm
Off-line wavelength	λ_{Off}	1572.11	nm
Receiver			
Type	Cassegrain telescope		
Area	A_r	1.77	m^2
Bandpass filter FWHM	$\Delta\lambda$	800	pm
Optical efficiency	η_0	80 %	-
FOV (full)	θ_{FOV}	50	µR
Detector			
Type	Multiple channel Geiger mode NFADs		
Detection efficiency	η_e	30 %	-
Detector dark count	N_{dc}	100	kcps
Miscellaneous			
Orbit type	6-h sun synchronous		
Solar zenith angle	θ_{zen}	75º	-
Ocean radiance	L_r	1.7	$mWm^{-2}nm^{-1}\ sr^{-1}$
Orbit altitude	R	450	km
Velocity	v	7	km/s
Surface albedo	α_S	0.03	sr^{-1}
On-line transmittance	T_{on}	0.3	-
Off-line transmittance	T_{off}	0.78	-
Number of 1s in the PRBS during averaging	m	$8.75\ 10^7$	-
Differential absorption optical depth	DAOD	0.48	-
CO_2 mixing ratio	XCO2	400	ppm

Table 2. Parameters used for SNR estimation for a space-borne RM-CW IPDA LIDAR.

V. SUMMARY

In this paper, we report on the progresses of the BRITESPACE Consortium in order to achieve space-borne LIDAR measurements of atmospheric carbon dioxide concentration based on an all semiconductor laser source at 1.57 µm. The complete design of the proposed RM-CW IPDA LIDAR has been presented and described in detail. Complete descriptions of the laser module and the FSU have been presented. Two bended MOPAs, emitting at the sounding frequency of the on- and off- IPDA channels, have been proposed as the transmitter optical sources with the required high brightness.

Experimental results on the bended MOPAs have been presented showing a high spectral purity and promising expectations on the high output power requirements. Finally, the RM-CW approach has been modelled and an estimation of the expected SNR for the entire system is presented. Preliminary results indicate that a CO_2 retrieval precision of 1.5 ppm could be achieved with an average output power of 2 W for each channel.

ACKNOWLEDGEMENT

This work was supported by the European Commission through the project BRITESPACE under grant agreement no. 313200.

REFERENCES

[1] http://www.britespace.eu/
[2] G. Ehret, et al., "Space-borne remote sensing of CO2, CH4, and N2O by integrated path differential absorption LIDAR: a sensitivity analysis," *Appl. Phys. B*, vol. 90, pp. 593-608, 2008.

[3] M. Quatrevalet, et al., "CHARM-F: The airborne integral path differential absorption lidar for simultaneous measurements of atmospheric CO_2 and CH_4," *in Proc. 25th Int. Laser Radar Conf.*, St. Peterburg, Russia, 2010.
[4] N. Takeuchi, N. Sugimoto, H. Baba, and K. Sakurai, "Random modulation cw lidar," *Appl. Opt.*, vol. 22, pp. 1382-1386, 1983.
[5] C. Nagasawa, M. Abo, H. Yamamoto, and O. Uchido, "Random modulation cw lidar using new random sequence," *Appl. Opt.*, vol. 29, pp. 1466-1470, 1990.
[6] X. Ai, R. Nock, J.G. Rarity, and N. Dahnoun, "High-resolution random-modulation cw lidar," *Appl. Opt.*, vol. 50, pp. 4478-4488, 2011.
[7] V. Mitev, R. Matthey, and D. Reusser, "Development of a pseudorandom noise modulation, continuous-wave (PRN-cw) total backscatter lidar," *in European Symposium on Optics for Environmental and Public Safety*. Munich, Germany, 1995.
[8] J.F. Campbell, B. Lin, and A.R. Nehrir, "Advanced sine wave modulation of continuous wave laser system for atmospheric CO2 differential absorption measurements," *Appl. Opt.,* vol. 53, pp. 816-829, 2014.
[9] E. Browell, S. Ismail, and W. Grant, "Differential absorption lidar (DIAL) measurements from air and space," *Appl. Phys. B.*, vol. 67, pp. 399-410, 1998.
[10] A. Fix, G. Ehret, J. Löhring, D. Hoffmann, and M. Alpers, "Water vapor differential absorption lidar measurements using a diode-pumped all-solid-state laser at 935 nm," *Appl. Phys. B,* vol. 102, pp. 905-915, 2011.
[11] K. Numata, J.R. Chen, S.T. Wu, J.B. Abshire, and M.A. Krainak, "Frequency stabilization of distributed-feedback laser diodes at 1572 nm for lidar measurements of atmospheric carbon dioxide," *Appl. Opt.*, vol. 50, pp. 1047-1056, 2011.
[12] B.P. Fox, K. Simmons-Potter, W.J. Thomes Jr., and D.A.V. Kliner, "Gamma-radiation-induced photodarkening in unpumped optical fibers doped with rare-earth constituents," *IEEE Trans. Nucl. Sci.*. vol. 57, pp. 1618-1625, 2010.
[13] X. Ai et al., "Pseudo-random single photon counting for space-borne atmospheric sensing applications" in *IEEE Aerospace Conference*, Big Sky, Montana, USA, 2014.
[14] M. Spreemann, M. Lichtner, M. Radziunas, U. Bandelow, and H. Wenzel, "Measurement and simulation of distributed feedback tapered master-oscillator power-amplifiers" *IEEE J. Quantum Electron.*, vol. 45, pp. 609–616, 2009.
[15] P. Adamiec, B. Bonilla, A. Consoli, J. M. G. Tijero, S. Aguilera, and I. Esquivias, "High-peak-power pulse generation from a monolithic master oscillator power amplifier at 1.5 μm," Appl. Opt., vol. 51, pp. 7160-7164, 2012.
[16] T. Kaminski, M. Scholze, and S. Houweling, "Quantifying the benefit of A-SCOPE data for reducing uncertainties in terrestrial carbon fluxes in CCDAS", *Tellus*, vol. 62B, pp. 784-796, 2010.